

## Research



**Cite this article:** Brely L, Bosia F, Palumbo S, Fraldi M, Dhinojwala A, Pugno NM. 2019 Competition between delamination and tearing in multiple peeling problems. *J. R. Soc. Interface* **16**: 20190388.  
<http://dx.doi.org/10.1098/rsif.2019.0388>

Received: 7 June 2019  
 Accepted: 30 October 2019

**Subject Category:**  
 Life Sciences—Physics interface

**Subject Areas:**  
 biomechanics, biomimetics

**Keywords:**  
 adhesion, fracture, multiple peeling, simulations, spider web

**Author for correspondence:**  
 Nicola M. Pugno  
 e-mail: [nicola.pugno@unitn.it](mailto:nicola.pugno@unitn.it)

# Competition between delamination and tearing in multiple peeling problems

Lucas Brely<sup>1</sup>, Federico Bosia<sup>1</sup>, Stefania Palumbo<sup>2</sup>, Massimiliano Fraldi<sup>2</sup>, Ali Dhinojwala<sup>3</sup> and Nicola M. Pugno<sup>4,5,6</sup>

<sup>1</sup>Department of Physics and 'Nanostructured Interfaces and Surfaces' Inter-Departmental Centre, Università di Torino, Via P. Giuria 1, 10125 Torino, Italy

<sup>2</sup>Department of Structures for Engineering and Architecture, University of Napoli Federico II, Naples, Italy

<sup>3</sup>Department of Polymer Science, The University of Akron, Akron, OH 44325-3909, USA

<sup>4</sup>Laboratory of Bio-Inspired and Graphene Nanomechanics, Department of Civil, Environmental and Mechanical Engineering, Università di Trento, via Mesiano, 77, I-38123 Trento, Italy

<sup>5</sup>School of Engineering and Materials Science, Queen Mary University of London, Mile End Road, London E1 4NS, UK

<sup>6</sup>Fondazione E. Amaldi, Ket Lab, Via del Politecnico snc, 00133 Rome, Italy

**ID** FB, 0000-0002-2886-4519; SP, 0000-0002-3242-3716; MF, 0000-0003-4164-8631; AD, 0000-0002-3935-7467; NMP, 0000-0003-2136-2396

Adhesive attachment systems consisting of multiple tapes or strands are commonly found in nature, for example in spider web anchorages or in mussel byssal threads, and their structure has been found to be ingeniously architected in order to optimize mechanical properties: in particular, to maximize dissipated energy before full detachment. These properties emerge from the complex interplay between mechanical and geometric parameters, including tape stiffness, adhesive energy, attached and detached lengths and peeling angles, which determine the occurrence of three main mechanisms: elastic deformation, interface delamination and tape fracture. In this paper, we introduce a formalism to evaluate the mechanical performance of multiple tape attachments in different parameter ranges, where an optimal (not maximal) adhesion energy emerges. We also introduce a numerical model to simulate the multiple peeling behaviour of complex structures, illustrating its predictions in the case of the staple-pin architecture. Finally, we present a proof-of-principle experiment to illustrate the predicted behaviour. We expect the presented formalism and the numerical model to provide important tools for the design of bioinspired adhesive systems with tuneable or optimized detachment properties.

## 1. Introduction

Spider silk is a biological fibrous material that displays exceptional mechanical properties [1] and comes in many different types, each with specific functions and properties [2]. Silk is the base construction material of spiders, and is used to fabricate complex structures such as the spider web. In addition to the main structure, the attachment between the silk threads and the substrate (figure 1*a*) plays an important role in determining the functionality of silk-based architectures. For example, it was shown that the contact, usually performed through adhesive-coated 'silken' threads called 'attachment discs' [3], differs in geometrical features depending on its prey-capture or locomotion functions [4]. To create a safe attachment between the dragline and the substrate, spiders create a structure referred to as a 'staple-pin' attachment. An array of perpendicular (or random, i.e. a disk) silken threads are used to 'coat' the main thread on which the external load is applied (figure 1*a*) [5]. When staple-pin structures are subjected to a peel test, different types of behaviour have been observed in natural systems [6]. The detachment occurs in some cases by delamination of the secondary tapes, which corresponds to the failure of the interface between the system and the substrate, and in other cases by the breakage of the secondary tapes themselves. The occurrence of these two mechanisms suggests that

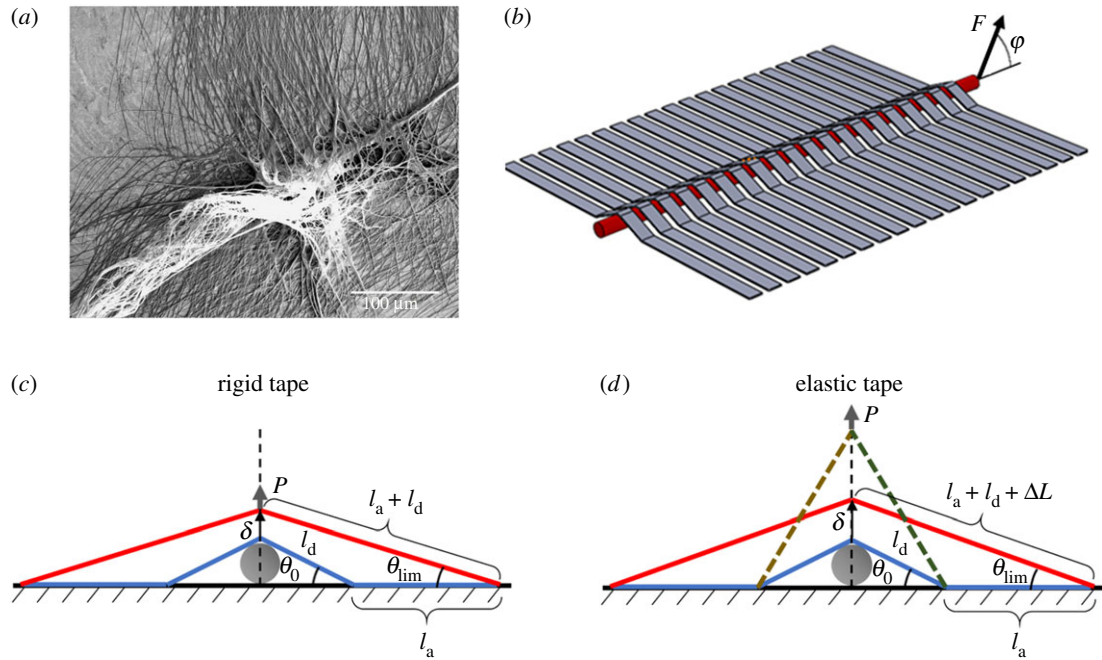


**Figure 1.** (a) Spider web anchorage; (b) schematic representation of a staple-pin attachment structure:  $F$  is the applied external load,  $\varphi$  its angle with respect to the substrate. (c,d) The symmetric double peeling system viewed as a sub-domain of the staple-pin in the rigid (c) and elastic (d) tape cases. In (d), the additional elastic deformation before delamination is illustrated with dashed lines.  $P$  is the applied load,  $l_a$  is the attached tape length,  $l_d$  is the detached tape length,  $\Delta L$  is the tape elongation,  $\delta$  is the vertical displacement of the load application point,  $\theta_0$  is the initial peeling angle,  $\theta_{lim}$  is the limit angle just before the full delamination of the tapes. (Online version in colour.)

the adhesive energy of the tape/substrate contact is high with respect to the fracture energy of the adhesive tapes, and that elastic deformation plays an important role in the total dissipated energy under the load of the staple-pin system. The compliance of the adhesive tapes, associated with a low contact angle in such structures has been attributed to a spider strategy to develop maximum adhesive strength out of a minimum amount of material and artificial systems mimicking the spider attachment disc have recently been introduced [7], with the aim of optimizing the maximum detachment force and the total dissipated energy out of minimal contact area and material use.

Various theoretical approaches have been developed to treat thin film peeling problems in the case of single [8,9] and multiple tapes [10]. The objective of the latter is to describe the behaviour of a system containing various simultaneously detaching tapes [11], which apply to natural systems like gecko toes [12] as well as spider web anchorages. However, the behaviour under the loading of multiple peeling systems is not trivial and *ad hoc* numerical procedures are required to simulate their delamination [13,14]. Various numerical approaches have been developed to address specific problems, such as adhesion to various types of surfaces [15], the influence of hierarchical structure [16], the role of friction [17] and viscoelasticity [18]. These numerical modelling tools are essential to design bioinspired artificial micro-patterned surfaces with optimized properties [19], including hierarchical structures [20].

Here, we develop analytical and numerical models to simulate the delamination and failure of coupled adhesive tapes, also taking into consideration the elastic deformation and the peeling angle variation under the load of the staple-pin attachment. We propose a general numerical scheme to model the detachment of staple-pin-like structures, introducing new aspects to existing models such as tape fracture and 3D deformation of the attachment devices.

## 2. Theoretical model

We consider the geometry shown in figure 1b. The attachment system is built from an array of tapes attached perpendicularly to the main cable on which a vertical external load is applied. Considering a single tape from the staple-pin structure, the problem reduces to studying the symmetric double peeling system shown in figure 1c,d [1]. As shown in the figure, for simplicity we consider the attached tape to be perfectly flat along its whole length, so that there is a discontinuity in its curvature at the location of the peeling line. This is an approximation whose validity decreases for increasing substrate softness or tape thickness.

The detachment of tapes adhering to a substrate can be theoretically described using Griffith's energy balance. The energy release rate during delamination can be defined as the instantaneous variation of potential energy  $\Pi$  per unit area  $A$ , i.e.  $G = -(d\Pi/dA)$ . The peeling front advances when  $G$  reaches the critical energy release rate

$$G = G_C. \quad (2.1)$$

Writing the total potential energy as  $\Pi = U_e - V$ , where  $U_e$  is the stored strain energy and  $V$  the work associated with the external load acting on the system, this amounts to

$$\frac{1}{w} \left( \frac{\partial V}{\partial l} - \frac{\partial U_e}{\partial l} \right) = G_C, \quad (2.2)$$

where  $l$  is the current detached length of the tape ( $l \leq l_a$ ) and  $w$  its width.

### 2.1. Rigid tape case

We first consider an inextensible film, in which the contribution of the stored elastic energy is neglected ( $U_e = 0$ ), which leads to the solution of the Rivlin equation [2]. According to the latter, delamination occurs when  $T = T_{del}$  and

$$T_{del}(1 - \cos \theta) = wG_C, \quad (2.3)$$

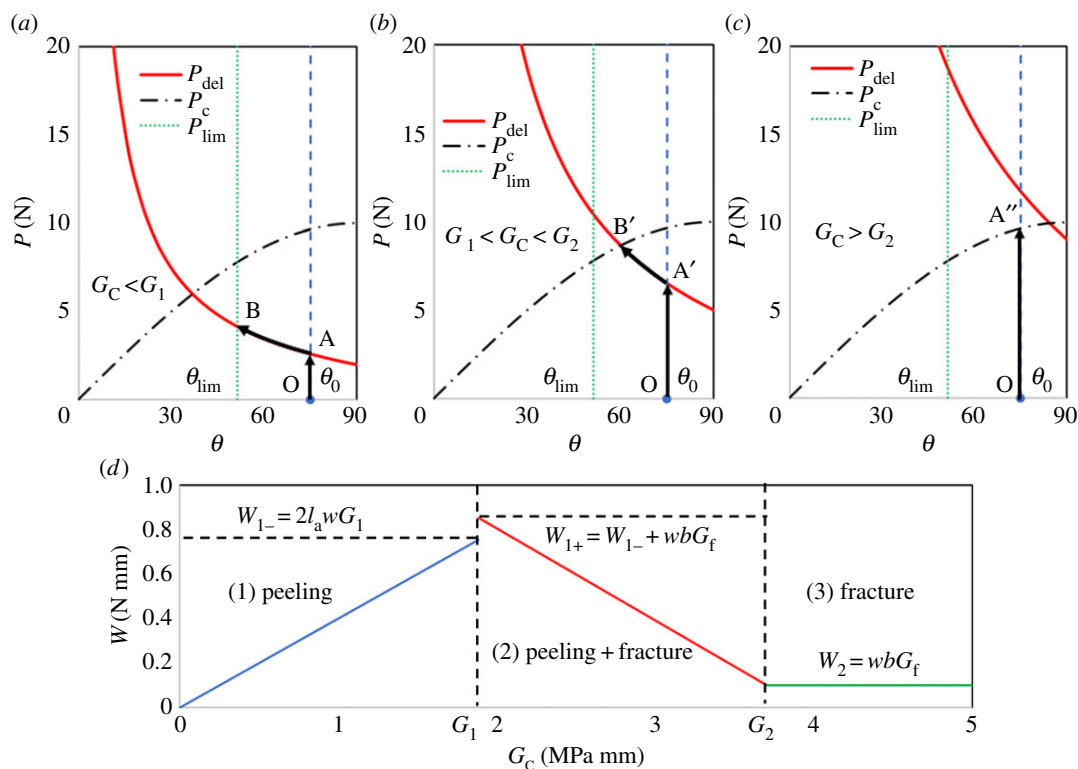


**Figure 2.** (a–c) External load  $P$  versus peeling angle  $\theta$  for rigid tape symmetric double peeling for increasing critical energy release rate  $G_C$ .  $P_{del}$  is the delamination load,  $P_c$  the critical (fracture) load,  $P_{lim}$  the load for complete delamination of the attached tape length  $l_a$ . (a)  $G_C < G_1$ : the tape delaminates over its entire attached length  $l_a$  until  $\theta = \theta_{lim}$  (path OAB); (b)  $G_1 < G_C < G_2$ : the tape delaminates and then fractures for  $P = P_c$  (path OA'B'); (c)  $G_C \geq G_2$ : the tape fractures before delamination at  $\theta = \theta_0$  (path OA''); (d) corresponding dissipated energy  $W$  versus  $G$ . (Online version in colour.)

where  $T$  is the tape tension,  $T_{del}$  is its critical value for delamination, and  $\theta$  is the peeling angle, i.e. the angle between the tape and the substrate. For the symmetric V-shaped double peeling system in figure 1c, the applied external load  $P$  is

$$P = 2 \sin \theta T, \quad (2.4)$$

and peeling starts when the external load reaches the value  $P_{del}$

$$P_{del}(\theta) = \frac{2wG_C \sin \theta}{1 - \cos \theta}. \quad (2.5)$$

Overall, from an initial tape-substrate angle configuration  $\theta_0$ , when the external load is applied, the peeling angle decreases as the structure detaches. This behaviour is shown in a  $P$  versus  $\theta$  plot in figure 2, for  $w = 1$  mm,  $\theta_0 = 75^\circ$  and three increasing  $G_C$  values: (a)  $G_C = 1$  kJ m $^{-2}$ , (b)  $G_C = 2.5$  kJ m $^{-2}$  and (c)  $G_C = 4.5$  kJ m $^{-2}$ . Starting from an unloaded structure ( $P(\theta_0) = 0$ , point O) and increasing  $P$ , the tapes will start to peel off at  $P = P_{del}$  (point A), leading to a decrease in the peeling angle and consequently an increase in  $P_{del}$ . In this case, the peeling angle tends to zero as the delamination proceeds and the peeling force increases indefinitely ( $P_{del} \rightarrow \infty$  for  $\theta \rightarrow 0$ ). The admissible space of load–angle configurations is  $\Omega = \{P \leq P_{del}\}$ .

We now introduce a critical tape tension  $T_c = \sigma_c b w$  at which the tape fractures, where  $\sigma_c$  is the tape strength and  $b$  the tape thickness. Depending on the adhesive energy and the geometrical and mechanical properties of the system, three different behaviours can occur as a function of the critical energy release rate  $G_C$  (figure 2). When  $G_C$  is smaller than a given value  $G_1$  ( $G_C < G_1$ , figure 2a), the tape delaminates over its full attached length  $l_a$  and the critical tension for fracture is not reached during the process. The limit angle before

complete delamination can be derived from geometrical considerations (figure 1c) as  $\cos \theta_{lim} = (l_d \cos \theta_0 + l_a) / (l_a + l_d)$ . Assuming now that the tape fractures immediately before reaching the peeling angle  $\theta_{lim}$ , we derive from equation (2.3) with  $T_{del} = T_c$

$$G_1 = \frac{T_c(1 - \cos \theta_{lim})}{w} = \frac{T_c(1 - \cos \theta_0)}{w} \frac{l_d}{l_a + l_d}. \quad (2.6)$$

If  $G_C$  is greater than a second given value  $G_2$  ( $G_C \geq G_2$ ) the tape fractures before any delamination (and thus angle change) occurs. This happens when the external load reaches a critical value  $P_c = 2 \sin \theta T_c$  (figure 2c). Again, from equation (2.3) with  $\theta = \theta_0$ , we have

$$G_2 = \frac{T_c(1 - \cos \theta_0)}{w} = \frac{l_a + l_d}{l_d} G_1. \quad (2.7)$$

If  $G_C$  lies between  $G_1$  and  $G_2$ , i.e.  $G_1 < G_C < G_2$ , the critical tension is reached after a finite delamination length (figure 2b).

The overall dissipated energy  $W$  depends on the energy release rate and the corresponding tape delamination behaviour, as well as the tape fracture energy

$$W = W_{del} + W_f, \quad (2.8)$$

where  $W_f = G_f b w$ , and  $G_f$  is the critical energy release rate for tape fracture. For full delamination with no fracture occurring for  $G_C < G_1$ , the dissipated energy increases linearly with  $G_C$ , i.e.  $W = 2l_a w G_C$  up to the value

$$W_{1-} = 2l_a w G_1. \quad (2.9)$$

If the critical energy release rate reaches the value  $G_C = G_1$ , the entire attached region peels off and the tape

fractures at the final delamination point (tape fracture is assumed to take place instantaneously). This corresponds to the maximum of dissipated energy, since tape fracture energy should be additionally considered

$$W_{1+} = 2l_a w G_1 + G_f b w. \quad (2.10)$$

For  $G_C$  values between  $G_1$  and  $G_2$ , the tape delaminates for part of its attached length and breaks when the applied load reaches  $P_c$ , with the dissipated energy  $W$  decreasing with delaminated tape length. Considering  $G_1 = G_C$  and  $l_a = l_c$  in equation (2.6), we can derive the delamination length  $l_c$  after which the tape breaks

$$l_c = l_d \left( 1 - \cos \theta_0 - \frac{w G_C}{T_c} \right) \frac{T_c}{w G_C}. \quad (2.11)$$

Thus, the dissipated energy for  $G_1 < G_C < G_2$  is

$$W = 2l_c w G_C + G_f b w = 2l_d T_c \left( 1 - \cos \theta_0 - \frac{w G_C}{T_c} \right) + G_f b w. \quad (2.12)$$

When  $G_C > G_2$ , the dissipated energy associated with delamination is zero, and only fracture energy remains, i.e.  $W_2 = G_f b w$ . The three cases are illustrated in figure 2d, where the dissipated energy is plotted as a function of the critical energy release rate adopting the test parameters  $l_d = l_a = 0.2$  mm,  $T_c = 5$  N and  $G_f = 10$  kJ m<sup>-2</sup>. The limit values  $G_1$  and  $G_2$  are both highlighted.

## 2.2. Elastic tape case

Considering now additionally tape elastic deformation and its contribution to energy balance (equation 2.2), equation (2.3) becomes the Kendall equation [9]

$$T_{\text{del}}(1 - \cos \theta) + \frac{T_{\text{del}}^2}{2Ewb} = w G_C, \quad (2.13)$$

where  $E$  is the tape elastic modulus. In this case, the peeling angle changes as a function of the elastic deformation and the detachment of the structure (figure 1d).

From a given initial configuration, it is possible to write the relationship between the tape strain  $\varepsilon$  and the tape-substrate angle  $\theta$  when the tape only deforms without detaching, as

$$l_d(1 + \varepsilon) \cos \theta = l_d \cos \theta_0. \quad (2.14)$$

Writing the tape tension as  $T_{\text{el}} = Ewb\varepsilon$ , we obtain

$$T_{\text{el}} = Ewb \left( \frac{\cos \theta_0}{\cos \theta} - 1 \right). \quad (2.15)$$

The external load  $P = P_{\text{el}}$  for the initial elastic deformation of the structure shown in figure 1d is therefore

$$P_{\text{el}}(\theta) = 2 \sin \theta T_{\text{el}} = 2 \sin \theta Ewb \left( \frac{\cos \theta_0}{\cos \theta} - 1 \right), \quad (2.16)$$

which for any given  $\theta$  assumes its maximal value for an initial peeling angle of  $\theta_0 = 0$ .

As discussed in multiple peeling theory [10], the overall delamination problem can be treated as the superposition of two independent single peeling processes, with each tape loaded by its peeling tension. The external load at delamination  $P_{\text{del}}$  for a given critical energy release rate  $G_C$  is

$$P_{\text{del}}(\theta) = 2 \sin \theta Ewb \left( \cos \theta - 1 + \sqrt{(1 - \cos \theta)^2 + \frac{2G_C}{Eb}} \right), \quad (2.17)$$

When  $P \geq P_{\text{del}}$ , delamination occurs. As discussed in [14], equation (2.15) is valid only for peeling angles  $\theta$  greater than the curve maximum occurring at  $\theta = \theta_{\text{max}}$ , which corresponds to an initial loading angle of  $\theta_0 = 0$ , since smaller  $\theta$  angles correspond to negative initial loading angles. From these considerations, we obtain the admissible space of load-angle configurations as  $\Omega = \{P(\theta) \leq P_{\text{del}}(\theta) \cap P(\theta) \leq P_{\text{el}}(\theta)\}$ .

The behaviour is shown in figure 3a–c, for test parameters  $w = 1$  mm,  $b = 0.01$  mm,  $E = 1$  GPa,  $l_d = 0.22$  mm,  $l_a = 1$  mm,  $\theta_0 = 75^\circ$ ,  $G_f = 5$  kJ m<sup>-2</sup> and three increasing  $G_C$  values: (a)  $G_C = 1.8$  kJ m<sup>-2</sup>, (b)  $G_C = 3$  kJ m<sup>-2</sup> and (c)  $G_C = 5$  kJ m<sup>-2</sup>. If the critical energy release rate is below  $G_1$ , for a given unloaded structure ( $P(\theta_0) = 0$ , point O), the system will first undergo elastic deformation without delamination (segment OA, along  $P = P_{\text{el}}$ ), and then both elastic deformation and delamination with a variable peeling angle (segment AB). The tape will then fully detach when its entire finite length delaminates at  $\theta = \theta_{\text{lim}}$  (point B). Alternatively, if  $l_a$  is sufficient for  $\theta_{\text{lim}}$  to reach  $\theta_{\text{max}}$ , the system will attain an equilibrium state where delamination proceeds at a constant peeling angle and load [14]. The corresponding peeling angle  $\theta_{\text{max}}$  can be derived by equating equation (2.16) for  $\theta_0 = 0$  and equation (2.17), leading to

$$2 \cos^3 \theta_{\text{max}} - \left( 3 + \frac{2G_C}{Eb} \right) \cos^2 \theta_{\text{max}} + 1 = 0, \quad (2.18)$$

whose (real) root can be obtained in closed form as

$$\cos \theta_{\text{max}} = \frac{(\beta - \alpha)[(1 - i\sqrt{3})\alpha - (1 + i\sqrt{3})\beta]}{12\beta}, \quad (2.19)$$

with  $\alpha = (3 + (2G_C/Eb))$  and  $\beta = \sqrt[3]{[\alpha^3 + 6(\sqrt{81 - 3\alpha^3} - 9)]}$ . In the case  $\theta_0 = 0$ , this equilibrium state would be reached as soon as the first delamination occurs. The more general case of  $\theta_{\text{lim}} < \theta_{\text{max}}$  is considered in figure 3a. Introducing, as for the rigid tape case, a fracture threshold  $T_c$ , for  $G_C = G_1$ , the tape fractures when it reaches  $\theta_{\text{lim}}$ . From geometrical considerations (figure 1c), since the tape elongation at fracture is  $\Delta L = T(l_a + l_d)/Ewb$ , we obtain

$$\cos \theta_{\text{lim}} = \frac{(l_a + l_d \cos \theta_0)/(l_a + l_d)}{(1 + T_c/Ewb)}, \quad (2.20)$$

which gives the correct  $\theta_{\text{lim}}$  value for the rigid tape case if  $E \rightarrow \infty$ .

When  $G_C = G_1$ ,  $T_{\text{del}} = T_c$  can be written as

$$T_c = Ewb \left( \cos \theta_{\text{lim}} - 1 + \sqrt{(1 - \cos \theta_{\text{lim}})^2 + \frac{2G_1}{Eb}} \right), \quad (2.21)$$

so that (also directly from Eq. (2.13))

$$G_1 = (1 - \cos \theta_{\text{lim}}) \frac{T_c}{w} + \frac{T_c^2}{2Ew^2b}, \quad (2.22)$$

which again gives the correct value provided in equation (2.6) for the rigid tape case ( $E \rightarrow \infty$ ). Notice that if  $\theta = \theta_{\text{max}}$  occurs for  $G_C < G_1$ , no tape fracture takes place, since delamination proceeds thereupon at a constant load.

For an increasing critical energy release rate ( $G_1 \leq G_C < G_2$ ), the tape deforms (segment OA'), then delaminates, and fractures in B' before the limit angle is reached (figure 3b). Finally, for  $G_C \geq G_2$  the tape deforms elastically and fractures in A'' before delamination starts (figure 3b). The value of  $G_2$  can be obtained from equation (2.13) for  $T_{\text{del}} = T_c$  combined

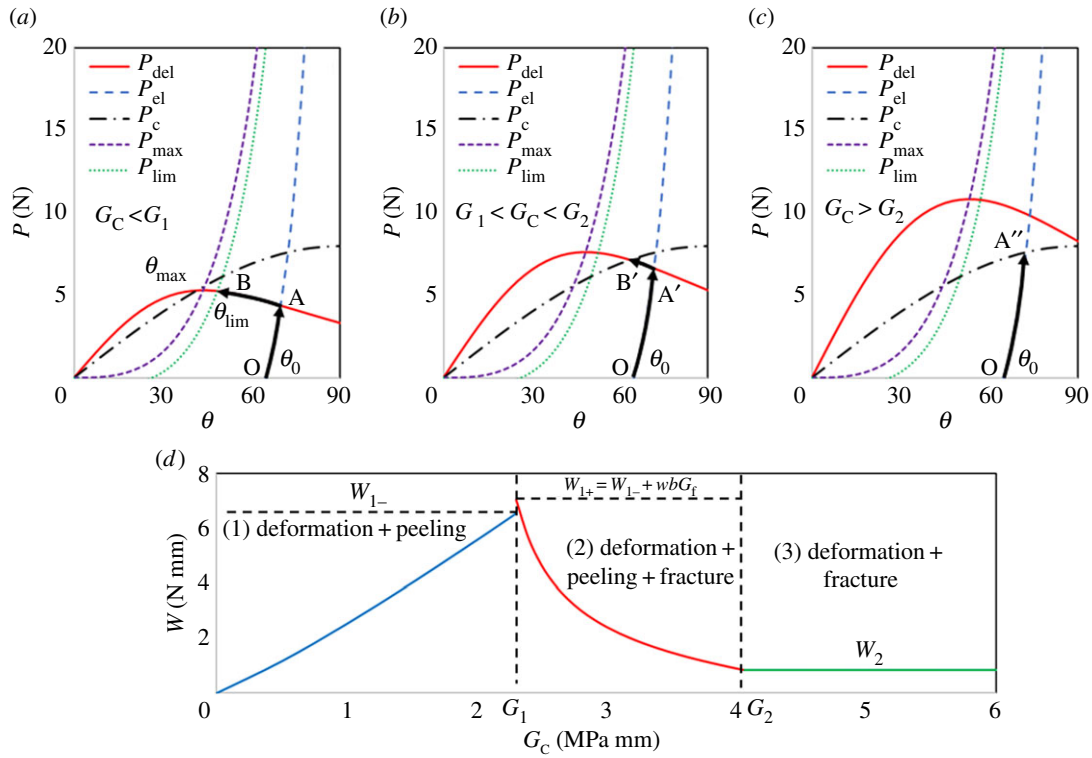


**Figure 3.** (a–c) External load  $P$  versus peeling angle  $\theta$  for elastic tape symmetric double peeling for increasing critical energy release rate  $G_C$ .  $P_{el}$  is the load for elastic deformation,  $P_{del}$  is the delamination load,  $P_c$  the critical (fracture) load,  $P_{max}$  the maximum peeling load,  $P_{lim}$  the load for complete delamination of the attached tape length  $l_a$ . (a)  $G_C < G_1$ : the tape deforms (path OA) and then delaminates (path AB) over  $l_a$  until  $\theta = \theta_{lim}$ ; (b)  $G_1 \leq G_C < G_2$ : the tape deforms (path OA'), delaminates (path A'B') and then fractures for  $P = P_c$ ; (c)  $G_C > G_2$ : the tape deforms (path OA'') and fractures before delamination for  $P = P_c$ . (d) Corresponding dissipated and released energy  $W$  versus  $G_C$ . (Online version in colour.)

with equation (2.15), giving

$$G_2 = \left(1 - \frac{\cos \theta_0}{(T_c/Ewb + 1)}\right) \frac{T_c}{w} + \frac{T_c^2}{2Ew^2b} \quad (2.23)$$

This expression tends to that in equation (2.7) for  $E \rightarrow \infty$ .

The dissipated and released energy  $W$  in the elastic tape case is the sum of the released elastic, delamination and fracture energies

$$W = U_{el} + W_{del} + W_f \quad (2.24)$$

where  $U_{el}$  is the elastic energy stored in the deformed tape when complete detachment or fracture occurs. Thus, for  $G_C < G_1$ ,  $W$  increases with  $G_C$  as

$$W = 2(l_a + l_d) \frac{T_{del}^2}{2Ewb} + 2l_a w G_C, \quad (2.25)$$

reaching a maximum value for  $T_{del} = T_c$  at  $W_{1-}$ , whereas  $W_{1+} = W_{1-} + wbG_f$  in  $G_1$ , where the additional tape fracture energy leads to a discontinuity in  $W$ . After this maximum value,  $W$  decreases with  $G_C$  as the delamination length decreases

$$W = 2(l_c + l_d) \frac{T_c^2}{2Ewb} + 2l_c w G_C + wbG_f, \quad (2.26)$$

where  $l_c$  is the delamination length before tape fracture, which can be deduced by inserting equation (2.20) with  $\theta_{lim} \rightarrow \theta$  and  $l_a \rightarrow l_c$  into equation (2.13) with  $T_{del} = T_c$ . Finally, the dissipated energy for  $G_C \geq G_2$  is constant and only due to the elastic deformation and fracture terms

$$W_2 = 2l_d \frac{T_c^2}{2Ewb} + wbG_f. \quad (2.27)$$

The load versus displacement curve in the optimal case  $W_{max} = W(G_C = G_1)$  is shown in figure 4, together with the contribution of the elastic and delamination energy, evaluating  $\delta$  geometrically from figure 1(d). The resulting curve displays an elastoplastic-like behaviour.

Notice that the above discussion can be generalized from a 2D to 3D structure, in which the deformed detached length of the tape is not aligned with the delamination direction, as illustrated in figure 5. In this case, equation (2.3) is modified as follows:

$$T_{del}(1 - \cos \theta \cos \lambda) = wG_C, \quad (2.28)$$

where  $\lambda$  is the angle defining the misalignment of the detached tape and attached length, due to deformation or initial conditions. Since the elastic energy variation and the surface energy remain unchanged, equation (2.13) becomes

$$T_{del}(1 - \cos \theta \cos \lambda) + \frac{T_{del}^2}{2Ewb} = wG_C. \quad (2.29)$$

When the attached and detached tapes are aligned ( $\lambda = 0$ ) the above equation coincides with equation (2.13). Solving equation (2.29) provides the tension needed to detach the tape

$$T_{del} = 2Ewb \left( \cos \theta \cos \lambda - 1 + \sqrt{(1 - \cos \theta \cos \lambda)^2 + \frac{2G_C}{Eb}} \right). \quad (2.30)$$

These equations are valid under the hypothesis that even when  $\lambda \neq 0$ , the load is equally distributed over the peeling line, and that the width of the peeling line remains unchanged (with respect to  $\lambda = 0$ ). This could be an oversimplification of the problem in some cases, and local load

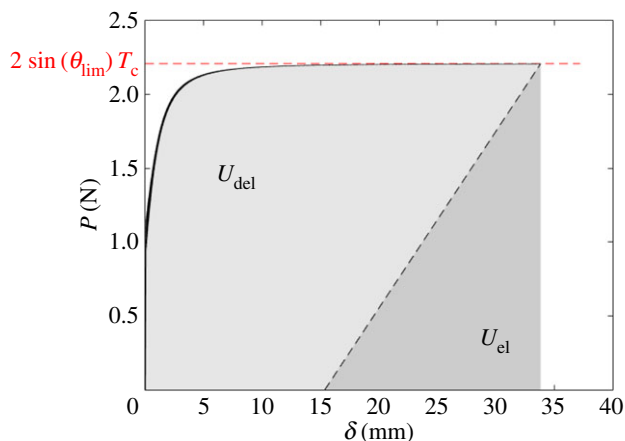


**Figure 4.** External load as a function of the displacement at the load application point during the detachment of a symmetric double peeling elastic tape when the adhesive energy is optimal. The energy dissipated during detachment and the stored elastic energy are shown as shaded areas. (Online version in colour.)

concentrations could appear, with a reduction of the peeling force.

### 3. Numerical implementation

To simulate the delamination and fracture behaviour of arbitrary multiple tape structures, we adopt a general numerical model based on mechanical equilibrium and energy balance [14]. For a given structure in 3D space, mechanical equilibrium is obtained using the co-rotational truss formulation [21].

The system is built using a frame of truss members sustaining axial load only, where the elements in contact with the substrate act as peeling tapes. The bending stiffness is, therefore, neglected. A member  $k$  of the system linking the nodes  $i$  and  $j$ , is defined by its initial length  $l$ , thickness  $b$ , width  $w$ , elastic modulus  $E$ . The stiffness  $k_k$  of the  $k$ th truss member in the local coordinate system (1D along the axis of the truss member) is

$$k_k = \frac{E_k b_k w_k}{l_k}. \quad (3.1)$$

The material stiffness of this element in the global coordinate system (3D) is obtained constructing the transformation vector

$$\mathbf{L} = [c_1 \quad c_2 \quad c_3 \quad -c_1 \quad -c_2 \quad -c_3] \quad (3.2)$$

where  $c_1$ ,  $c_2$  and  $c_3$  are the element direction cosines in 3D space

$$c_1 = \frac{x_j - x_i}{l_k}, \quad (3.3)$$

$$c_2 = \frac{y_j - y_i}{l_k}, \quad (3.4)$$

and 
$$c_3 = \frac{z_j - z_i}{l_k}, \quad (3.5)$$

and  $\mathbf{x} = [x \quad y \quad z]$  is the coordinate vector of a node under the deformation of the system. The material stiffness matrix  $\mathbf{K}_m$  is then written as

$$\mathbf{K}_m = k_k \mathbf{L}^T \mathbf{L}. \quad (3.6)$$

The external force vector  $\mathbf{Q}_e$  contains the components of the external load acting on the system. Rather than directly

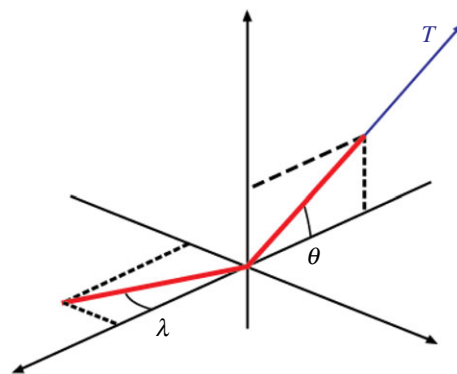


**Figure 5.** Misalignment between the attached and detached tape. (Online version in colour.)

solving the linear system in terms of nodal displacements  $\mathbf{K}_m \mathbf{u} = \mathbf{Q}_e$ , an iterative scheme is implemented to address the geometrical nonlinearity arising from this type of mechanical system. Indeed, large rotations of the truss members are expected, which need to be taken into account in order to obtain an accurate displacement field. We introduce the geometric stiffness matrix as

$$\mathbf{K}_g = \frac{k_k \delta l_k}{l_k + \delta l_k} \mathbf{H}, \quad (3.7)$$

where  $\delta l_k$  is the elongation of the deformed element,  $\mathbf{H} = \mathbf{h}^T \mathbf{h}$ ,  $\mathbf{h} = [-\mathbf{I} \quad \mathbf{I}]$  and  $\mathbf{I}$  is the identity matrix. The truss member contribution to the internal force vector is

$$\mathbf{Q}_i = k_k \delta l_k \mathbf{L}^T. \quad (3.8)$$

Once all contributions are assembled in the linear system, mechanical equilibrium is obtained by updating the nodal displacement according to the following iterative scheme

$$\mathbf{u} + (\mathbf{K}_m + \mathbf{K}_g)^{-1} (\mathbf{Q}_e - \mathbf{Q}_i) \rightarrow \mathbf{u}. \quad (3.9)$$

The 2-norm of the residual  $\|\mathbf{Q}_e - \mathbf{Q}_i\|$  is used as convergence criterion. Therefore, the equilibrium between internal and external loads is verified, including in the case of large rotations.

In order to control the tape delaminations, the external load is incremented iteratively, and the total potential energy variation is calculated at each increment. The delamination of a discrete length  $\Delta l$  of a member in contact with the substrate leads to a modification of its length (and therefore its stiffness) and of the coordinates of the node in contact

$$l + \Delta l \rightarrow l \quad (3.10)$$

and

$$\mathbf{x} + \Delta \mathbf{x} \rightarrow \mathbf{x}. \quad (3.11)$$

The change in the attached node coordinate depends on the direction of the attached part of the delaminating tape respect to the detached one. It has two components on the  $x$ - $y$  substrate plane and a zero value in the  $z$ -direction ( $\Delta l = \sqrt{\Delta x^2 + \Delta y^2}$ ). At each step of the simulation, the energy variation is verified for all the members in contact, between the current state (a) and the state where the considered tape detachment has been incremented (b). The external work variation associated with the detachment of the tape  $k$  is the 1-norm of the product of the external force

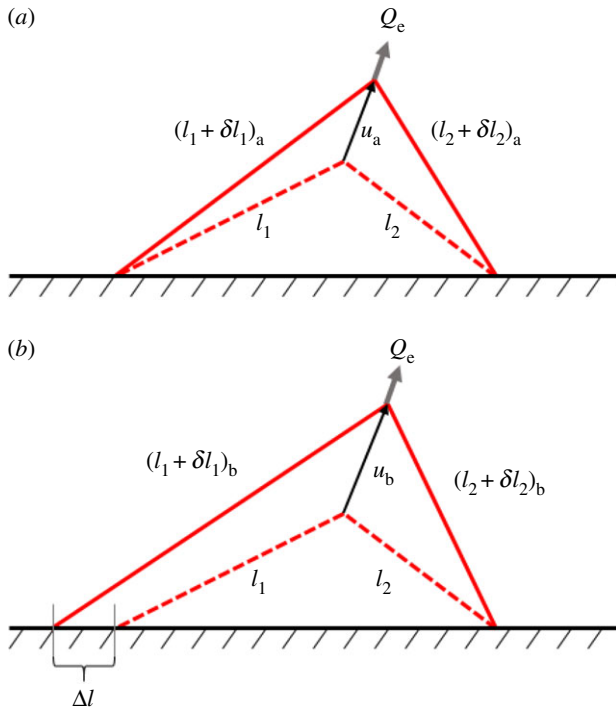


**Figure 6.** (a) Current deformed state (state a) of a V-shape 2D attachment system under load. (b) Increment in the first tape detached length. (Online version in colour.)

vector and the difference between displacement after and before detachment, i.e.

$$\frac{\Delta V}{\Delta l} = |\mathbf{Q}_{\text{ext}}(\mathbf{u}_b - \mathbf{u}_a)|. \quad (3.12)$$

The variation of elastic energy in the system is obtained as

$$\frac{\Delta U_e}{\Delta l} = \frac{1}{2} \sum_{k=1}^N [(k_k \delta l_k^2)_b - (k_k \delta l_k^2)_a], \quad (3.13)$$

where  $N$  is the total number of truss members in the system. Detachment occurs, according to equation (2.2), when

$$\frac{\Delta V}{\Delta l} - \frac{\Delta U_e}{\Delta l} \geq wG_C. \quad (3.14)$$

Figure 6 illustrates the method used to check whether a tape has delaminated or not for a simple V-shaped tape system observed in the  $x$ - $z$  plane. The displacement field of the system as a response to the external load is first computed (figure 6a). Then, for each element in contact with the substrate, the detached length of the element is incremented and the tape length and its attached node coordinates updated. The new displacement field is then computed to test if the element has delaminated, as shown in figure 6b for the first element delamination test. We then check if detachment has occurred by calculating the variation of potential energy in (3.14). If not, the system is reset and the next element delamination is verified. If no delamination is observed, the external load is incremented, and so on until the whole system has been fully detached.

Tape fracture is introduced by a simple removal rule when one of the tape tensions reaches the critical value  $T_c$ . If the tape geometry and loading are in the same plane, the system can be reduced to a 2D problem.

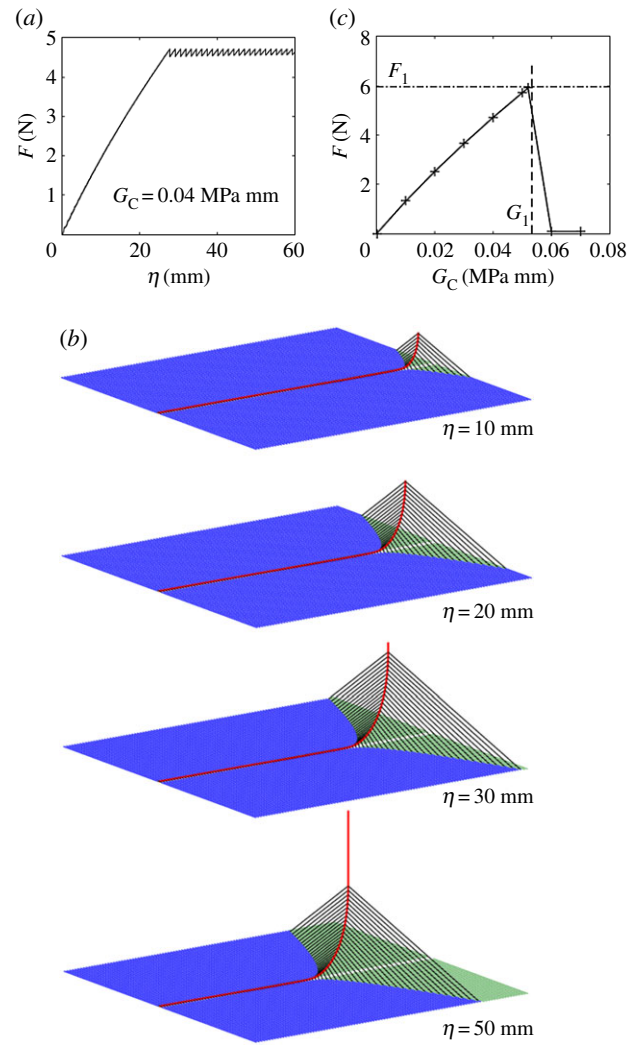


**Figure 7.** (a) External load to the displacement of the load application point during detachment of the staple-pin structure obtained from the numerical model. (b) Corresponding evolution of the system (the red line is the cable, the black lines are the detached tape regions, the blue lines are the attached tape regions and the green lines are the detachment path of the adhesive tapes. The fully detached tapes are not represented). (c) Overall detachment force as a function of the adhesive energy obtained from the numerical model, plotted together with the theoretical optimal. (Online version in colour.)

## 4. Numerical results

We use the previously described numerical method to model the complete staple-pin system shown in figure 1. The drag-line, or cable that supports the external load is assumed to have a diameter  $d^* = 0.2$  mm with a circular cross-section  $A^* = \pi d^{*2}/4$ , an elastic modulus  $E^* = 100$  MPa and a length  $L_0 = 100$  mm, for a total number of  $n = 50$  transversal tapes with a spacing  $s = 1$  mm. We assume for each of these tapes the following properties:  $w = 1$  mm,  $b = 0.01$  mm,  $E = 100$  MPa,  $l_a = 50$  mm,  $\theta_0 = \pi/16$ ,  $l_d = d^*/\sin \theta_0$  and  $T_c = 0.2$  N. An example of the global load  $F$  vs. displacement  $\eta$  response, together with the evolution of the deformed and peeled system is shown in figure 7.

We first consider the case in which the critical energy release rate  $G_C$  is small enough for the system to completely peel-off over its entire attached regions without any fracture ( $G_C = 0.04 \text{ kJ m}^{-2} < G_1 = 0.05 \text{ kJ m}^{-2}$ ), applying a load perpendicular to the substrate at  $\varphi = \pi/2$ . The corresponding

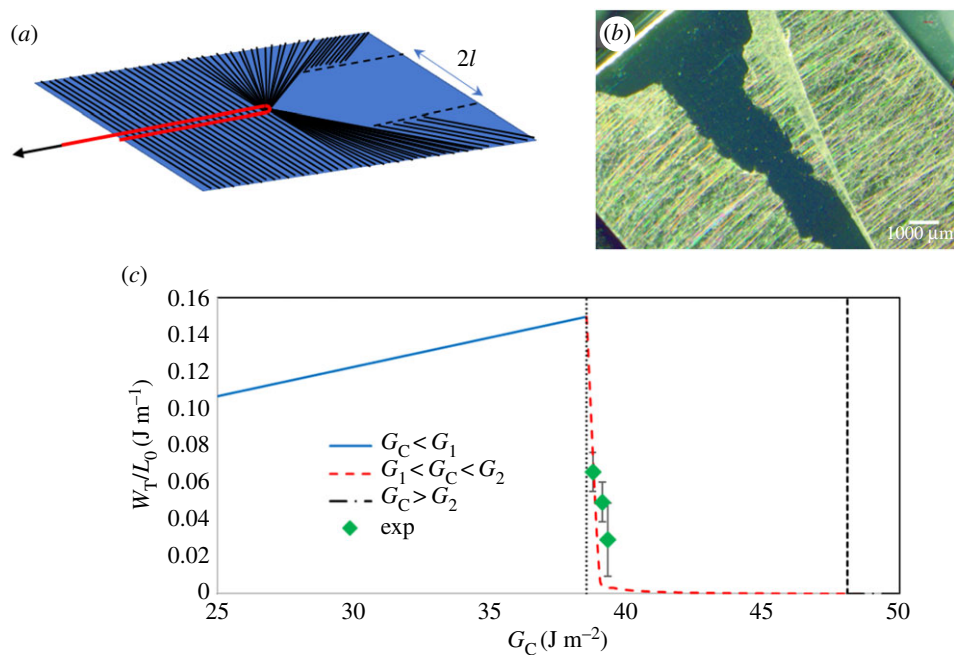


**Figure 8.** (a) Schematic of experimental test, with staple-pin architecture pulled at  $\varphi = \pi$ ; (b) optical image of the peeling behaviour of a disc prepared on an oxygen-plasma treated substrate: the peeling starts with a w-shaped zone but proceeds with delamination over a relatively uniform width; (c) comparison between model predictions and experimental data for dissipated energy per unit disc length  $L_0$  as a function of the critical energy release rate. (Online version in colour.)

overall load–displacement curve is shown in figure 7a, displaying an initial quasi-linear behaviour, and then a constant-load plastic-like branch, where an equilibrium is reached as the secondary transversal tapes are delaminating. The whole structure detaches at approximately constant load, apart from small oscillations in the force value due to the delaminating tapes. Various snapshots of the deformation profile of the entire structure as it delaminates are shown in figure 7b, highlighting the advancing delamination front as the load application point displacement increases. The overall adhesive force  $F$  as a function of the critical energy release rate is shown in figure 7c, again for an external load perpendicular to the substrate  $\varphi = \pi/2$ . This highlights the discussed transition from delamination to fracture behaviour of the tapes at  $G_1 = 0.05 \text{ kJ m}^{-2}$ . This value coincides with the optimal critical energy release rate predicted with equation (2.22).

To analytically predict the global peeling force, energy balance expressed in equation (2.2) can be applied to the cable. The interaction between the cable and the substrate occurs through the transversal tapes, each of which can dissipate a total amount of energy  $W$  given by equation (2.24). Dividing this value by the width of the tapes gives the energy per unit length needed to detach the cable. Using equation (2.13), the energy balance applied directly to the cable becomes

$$F(1 - \cos \varphi) + \frac{F^2}{2E^*A^*} = \frac{W}{s}. \quad (4.1)$$

Thus, the global peeling force becomes

$$F = 2E^*A^* \left( \cos \varphi - 1 + \sqrt{(1 - \cos \varphi)^2 + \frac{2W}{sE^*A^*}} \right). \quad (4.2)$$

Comparing the maximum peeling force obtained in the simulations with the theoretical one (indicated as  $F_1$ ) in

equations (2.25) and (4.2), a good agreement is found (figure 7c).

## 5. Experimental validation

To further verify the validity of the presented model, a comparison is made with experimental results from [7], where artificial staple-pin attachment discs were fabricated through electrospinning and tested in peeling experiments on aluminium substrates with variable adhesive characteristics. As schematically shown in figure 8a, a  $30 \mu\text{m}$ -diameter nylon fibre was pulled at a peeling angle of  $\varphi = \pi$ , leading to the delamination, deformation and fracture of perpendicularly placed polyurethane fibres. Typically, this leads to a delamination zone of relatively constant width, as shown in figure 8b. Having derived single fibre tensile properties up to fracture, it was, therefore, possible to estimate for each tested attachment disc the dissipated energy in peeling and in deformation up to fracture, as described in [7]. The larger the delaminated width ( $2l_c$ , see Section 2), the larger the dissipated energy. Three different substrate adhesive properties were considered, i.e. a perfluoro-plasma treated aluminium substrate, an untreated substrate, and an oxygen-plasma treated aluminium substrate (in order of increasing adhesive properties). This allows us to compare model predictions to experimentally measured points.

A single polyurethane fibre in the staple-pin structure has a diameter of  $1.5 \mu\text{m}$  and an initial detached length approximately equal to the radius of the nylon fibre:  $l_d = 15.0 \mu\text{m}$ . Its Young's modulus  $E$  and critical tension  $T_c$  are derived from tensile tests as  $E = 10.7 \text{ MPa}$  and  $T_c = 39.9 \mu\text{N}$ . The spacing between fibres is approximately  $s = 15 \mu\text{m}$ . The average delaminated lengths before fracture for the three considered substrates are  $l_{c1} = 2.01 \text{ mm}$ ,  $l_{c2} = 1.71 \text{ mm}$ ,  $l_{c3} = 0.45 \text{ mm}$ . Since in all three cases fracture takes place after the transversal fibres have partially delaminated, the experimental

scenario corresponds to the case  $G_1 < G_C < G_2$ . The  $G_C$  values of the three experimental points are determined from their delaminated length values  $l_{ci}$ , determined as explained previously in §2.2 (after equation (2.26)) giving:

$$l_c = l_d \frac{1 - \cos \theta_0 - \left( \frac{wG_C}{T_c} - \frac{T_c}{2Ewb} \right) \left( 1 + \frac{T_c}{Ewb} \right)}{\left( \frac{wG_C}{T_c} - \frac{T_c}{2Ewb} \right) \left( 1 + \frac{T_c}{Ewb} \right)}. \quad (4.3)$$

The total dissipated energy per unit length of the nylon fibre  $L_0$  can be derived by taking the integral of the experimental force/displacement curves and dividing them by  $L_0$ , and corresponds in the three cases to average values of  $W_{T1}/L_0 = 0.065 \text{ J m}^{-1}$ ,  $W_{T2}/L_0 = 0.050 \text{ J m}^{-1}$ ,  $W_{T3}/L_0 = 0.029 \text{ J m}^{-1}$ . These values are obtained at a collector velocity of  $0.1 \text{ cm s}^{-1}$  and peeling rate of  $1 \text{ mm s}^{-1}$ . Rate effects are not considered/modelled in this work.

These experimental values can be compared to theoretical values, using the system geometrical and mechanical parameters: first,  $\cos \theta_{im}$  is calculated from equation (2.20) (using the entire nylon fibre diameter to estimate  $w$  of the polyurethane fibres), and from it,  $G_1$  and  $G_2$  using equations (2.22) and (2.23). Then, the corresponding dissipated energy per unit length is derived using equation (2.26), as  $W_T/L_0 = W/s$ .

Results are shown in figure 8c, in terms of dissipated energy (per unit length  $L_0$ ) as a function of critical energy release rate, having assumed for simplicity  $\theta_0 \sim \pi/2$ . The experimental data are compatible with the model predictions, i.e. the total energy dissipated during peeling is found to be higher for surfaces with smaller work of adhesion [7]. This results in a larger volume of threads getting deformed during peeling, and in higher total energy dissipated during the peeling process.

## 6. Discussion

Numerical and experimental data confirm model predictions that the global adhesive force of the system is obtained from the energy dissipated by discrete sub-regions rather than from the maximum force they can carry. This has non-trivial consequences. Spiders employ multiple types of silks with different moduli and architecture to maximize the total work during attachment, rather than maximizing the maximum detachment force. For example, viscid silk threads used for capturing flying or walking prey use stretch flagilliform silk threads coated with glue droplets [4,22]. During peeling the glue droplets stretch and results in the formation of a suspension bridge-like structure, with the force distributed over a much larger volume of the silk thread [23]. This again results in maximizing the total energy dissipated during peeling as a result of stretching the flagilliform thread and multiple glue droplets, in addition to the thermodynamic work of adhesion.

In the case of pyriform attachment disks, recent work has highlighted how these structures are particularly efficient in providing high pull-off resistance, as well as being robust, given the large variation in the pulling angles occurring in a real environment [5]. Also, it has been shown that the silk anchor structure evolved and was optimized over millions of years, with considerable effects on the robustness of web attachment [24]. The large adhesion energy of the attachments prevents the threads from peeling and this results in less energy spent in stretching the peeled threads. Therefore, the total energy involved in peeling is reduced.

Additionally, in biological adhesion, typical structures often display a hierarchical architecture, which means that energy dissipation mechanisms occur at different scale levels simultaneously, each of them having a specific response to different load distributions over its sub-units. At present, most of the studies are focused on the detachment force of the contact units [25]. The present work shows that from a lower to an upper level, the dissipated energy of each contact is more important than its maximum detachment force. This is particularly important in cases in biological adhesion where most of the contacts are realized using tape-like units, displaying a typical 'elastoplastic' behaviour such as that shown in figure 4, where the maximum detachment force is not sufficient to determine the total dissipated energy.

## 7. Conclusion

We have studied fibrous or tape-like attachment systems with multiple contacts, such as those found in staple-pin structures in spider webs, introducing a general analytical scheme that includes both delamination and tape fracture, and validating it with numerical simulations and experimental data. We have shown that adhesive energy and mechanical strength are synergetic in providing optimized load-bearing properties, i.e. the maximum load an attachment can support before detachment. Additionally, we have shown that the energy dissipated by the contacts, accounting for elastic deformation, detachment and fracture, determines the adhesive force of a multiple peeling system.

Since structures formed by arrays of contact units, usually tape-like contacts, are recurrent in biological adhesives, the model discussed could help to improve the understanding of Nature's strategies to enhance and optimize adhesion. This approach could also be useful in the future for the design and optimization of artificial bioinspired adhesives, maximizing adhesive strength while minimizing material use.

**Data accessibility.** This article has no additional data.

**Authors' contributions.** L.B. performed numerical simulations and prepared the first draft. F.B. supervised the work, compared experimental data to theoretical predictions, and wrote the revised manuscript. S.P. and M.F. helped with the theoretical formulation. A.D. provided the original idea and experimental data. N.M.P. supervised the work, provided the original idea and the rigid tape theoretical model, and corrected the manuscript.

**Competing interests.** We declare we have no competing interests.

**Funding.** F.B. is supported by H2020 FET Proactive 'Neurofibres' grant no. 732344, by the project 'Metapp' (no. CSTO160004) funded by Fondazione San Paolo, and by the Italian Ministry of Education, University and Research (MIUR), under the 'Departments of Excellence' grant L. 232/2016. M.F. is supported by Regione Campania under the CIRO (Campania Imaging Infrastructure for Research in Oncology) and SATIN (Therapeutic Strategies against Resistant Cancer) grants and by the Italian Ministry of Education, University and Research (MIUR) under the ARS01-01384-PROSCAN and the PRIN-20177TTP3S grants. N.M.P. is supported by the European Commission under the Graphene Flagship Core 2 grant no. 785219 (WP14 'Composites') and FET Proactive 'Neurofibres' grant no. 732344 as well as by the Italian Ministry of Education, University and Research (MIUR) under the 'Departments of Excellence' grant no. L. 232/2016, the ARS01-01384-PROSCAN grant and the PRIN-20177TTP3S.

**Acknowledgements.** This work was carried out within the COST Action CA15216 'European Network of Bioadhesion Expertise: Fundamental Knowledge to Inspire Advanced Bonding Technologies'. Computational resources were provided by the C3S centre at the University of Torino (c3s.unito.it) and by hpc@polito (www.hpc.polito.it).

- Nova A, Keten S, Pugno NM, Redaelli A, Buehler MJ. 2010 Molecular and nanostructural mechanisms of deformation, strength and toughness of spider silk fibrils. *Nano Lett.* **10**, 2626–2634. (doi:10.1021/nl101341w)
- Cranford SW, Tarakanova A, Pugno NM, Buehler MJ. 2012 Nonlinear material behaviour of spider silk yields robust webs. *Nature* **482**, 72–76. (doi:10.1038/nature10739)
- Wolff JO, Grawe I, Wirth M, Karstedt A, Gorb SN. 2015 Spider's super-glue: thread anchors are composite adhesives with synergistic hierarchical organization. *Soft Matter* **11**, 2394–2403. (doi:10.1039/C4SM02130D)
- Sahni V, Harris J, Blackledge TA, Dhinojwala A. 2016 Cobweb-weaving spiders produce different attachment discs for locomotion and prey capture. *Nat. Commun.* **3**, 1106. (doi:10.1038/ncomms2099)
- Wolff JO, Herberstein M. 2017 Three-dimensional printing spiders: back-and-forth glue application yields silk anchorages with high pull-off resistance under varying loading situations. *J. R. Soc. Interface* **14**, 20160783. (doi:10.1098/rsif.2016.0783)
- Ingo G, Wolff JO, Gorb SN. 2014 Composition and substrate-dependent strength of the silken attachment discs in spiders. *J. R. Soc. Interface* **11**, 20140477. (doi:10.1098/rsif.2014.0477)
- Jain D, Sahni V, Dhinojwala A. 2014 Synthetic adhesive attachment discs inspired by spider's pyriform silk architecture. *J. Polym. Sci. B Polym. Phys.* **52**, 553–560. (doi:10.1002/polb.23453)
- Rivlin RS. 1997 The effective work of adhesion. In *Collected papers of RS Rivlin*, pp. 2611–2614. New York, NY: Springer.
- Kendall K. 1975 Thin-film peeling—the elastic term. *J. Phys. D Appl. Phys.* **8**, 1449. (doi:10.1088/0022-3727/8/13/005)
- Pugno NM. 2011 The theory of multiple peeling. *Int. J. Fract.* **171**, 185–193. (doi:10.1007/s10704-011-9638-2)
- Bosia F, Colella S, Mattoli V, Mazzolai B, Pugno NM. 2014 Hierarchical multiple peeling simulations. *RSC Adv.* **4**, 25 447–25 452. (doi:10.1039/C4RA03459G)
- Yao H, Gao H. 2006 Mechanics of robust and releasable adhesion in biology: bottom-up designed hierarchical structures of gecko. *J. Mech. Phys. Solids.* **54**, 1120–1146. (doi:10.1016/j.jmps.2006.01.002)
- Özdemir İ. 2017 A numerical solution framework for simultaneous peeling of thin elastic strips from a rigid substrate. *Acta Mech.* **228**, 1735–1747. (doi:10.1007/s00707-016-1796-x)
- Brely L, Bosia F, Pugno N. 2015 Numerical implementation of multiple peeling theory and its application to spider web anchorages. *Interface Focus* **5**, 20140051. (doi:10.1098/rsfs.2014.0051)
- Brely L, Bosia F, and Pugno N. 2017 The influence of substrate roughness, patterning, curvature and compliance in peeling problems. *Bioinspir. Biomim.* **13**, 026004. (doi:10.1088/1748-3190/aaa0e5)
- Brely L, Bosia F, Pugno N. 2018 Emergence of the interplay between hierarchy and contact splitting in biological adhesion highlighted through a hierarchical shear lag model. *Soft Matter* **14**, 5509–5518. (doi:10.1039/C8SM00507A)
- Braun OM, Barel I, Urbakh M. 2009 Dynamics of transition from static to kinetic friction. *Phys. Rev. Lett.* **103**, 194301. (doi:10.1103/PhysRevLett.103.194301)
- Lorenz B, Krick B, Mulakaluri N, Smolyakova M, Dieluweit S, Sawyer W, Persson BN. 2013 Adhesion: role of bulk viscoelasticity and surface roughness. *J. Phys. Condens. Matter* **25**, 225004. (doi:10.1088/0953-8984/25/22/225004)
- Northen MT, Greiner C, Arzt E, Turner KL. 2008 A gecko-inspired reversible adhesive. *Adv. Mater.* **20**, 3905–3909. (doi:10.1002/adma.200801340)
- Brodoceanu D, Bauer C, Kroner E, Arzt E, Kraus T. 2016 Hierarchical bioinspired adhesive surfaces—a review. *Bioinspir. Biomim.* **11**, 051001. (doi:10.1088/1748-3190/11/5/051001)
- Crisfield MA, Moita GF. 1996 A co-rotational formulation for 2-D continua including incompatible modes. *Int. J. Numer. Methods Eng.* **39**, 2619–2633. (doi:10.1002/(SICI)1097-0207(19960815)39:15<2619::AID-NME969>3.0.CO;2-N)
- Amarpuri G, Zhang C, Diaz C, Opell B, Blackledge T, Dhinojwala A. 2015 Spiders tune glue viscosity to maximize adhesion. *ACS Nano* **9**, 11 472–11 478. (doi:10.1021/acsnano.5b05658)
- Opell DB, Dhinojwala JA, Blackledge T. 2018 Tuning orb spider glycoprotein glue performance to habitat humidity. *J. Exp. Biol.* **221**, jeb161539. (doi:10.1242/jeb.161539)
- Wolff JO *et al.* 2019 Evolution of aerial spider webs coincided with repeated structural optimization of silk anchorages. *Evolution* **73**, 2122–2134. (doi:10.1111/evo.13834)
- Tian Y *et al.* 2006 Adhesion and friction in gecko toe attachment and detachment. *Proc. Natl Acad. Sci. USA.* **103**, 19 320–19 325. (doi:10.1073/pnas.0608841103)